Fiber-Optic Grid Interferogram Shape Sensing System

Libo Yuan, Yanlei Liu, Zhihai Liu, and Xiaoyan Lin

***Abstract*—Based on the three-fiber-optic grid interferogram technique, a shape sensing approach has been proposed and demonstrated in this paper. The square and hexagon grid interferometric fringe pattern formed by the fiber-optic interferometric grid generator has been designed and performed. The designing and realizing methods of the fiber-optic interferometric grid pattern by using three PM fibers are discussed. Theoretically, the three-fiber coherence optical field intensity distribution has been deduced. By using the 2-D Fourier transform methodology, the object surface can be reconstructed from the modulated fiber-optic grid interferogram pattern. The multiphase data fusion method has been used in our experiments, which greatly improved the accuracy of the 3-D shape measuring results.**

***Index Terms*—Fiber-optic grid interferogram, Fourier transform, optical fiber, shape sensing.**

I. Introduction

OPTICAL 3-D noncontact profilometry has been widely used for 3-D sensing, mechanical engineering, machine vision, intelligent robots control, industry monitoring, biomedicine, dressmaking, etc. Several 3-D object profilometry methods that use structured light pattern, including Moiré technique [1], [2], phase measuring profilometry [3]–[11], Fourier transformation profilometry [12], [13], and modulation measurement profilometry [14], [15] have been exhaustively studied.

This paper describes a shape sensing approach based on the use of the fiber-optic interferometric technique. The square and hexagonal carrier interference grid patterns are generated by three single-mode PM fibers. The fast 2-D Fourier transform method is used to process the modulated grid pattern: it extracts phase from grid patterns resulting from the interference of deformation wavefronts modulated by the shape of measured object. The shape sensing approach is illustrated by a 3-D shape measuring of uniformly optical grid pattern modulated by a triangle pyramid.

II. Generation of Square and Hexagonal Interference Grid Patterns

The fiber-optic based interference grid pattern generator is configured by three PM fibers. From the front view of the three PM fiber ends, its relative positions are shown in Fig. 1(a) and the three fiber ends output optical fields polarization directions are shown in Fig. 1(b). The coordinates of the three fibers core center position are $F_1(0,0), F_2(a,b)$ and $F_3(c,d)$, and the orientation angles of the three fibers output optical field polarization state can be described by θ_1, θ_2, and θ_3, respectively. The interference intensity in the observation plane (as shown in Fig. 2) was given by [16], [17]

$$
\begin{aligned}
I(x,y) &= I_1 + I_2 + I_3 \\
&\quad + 2\sqrt{I_1 I_2}\cos(\theta_1-\theta_2)\cos\left\{\frac{2\pi}{\lambda D}(ax+by)-\delta_{21}\right\} \\
&\quad + 2\sqrt{I_1 I_3}\cos(\theta_1-\theta_3)\cos\left\{\frac{2\pi}{\lambda D}(cx+dy)-\delta_{31}\right\} \\
&\quad + 2\sqrt{I_2 I_3}\cos(\theta_2-\theta_3)\cos\left\{\frac{2\pi}{\lambda D}[(c-a)x \right. \\
&\quad \left. + (d-b)y]-\delta_{32}\right\} \qquad (1)
\end{aligned}
$$

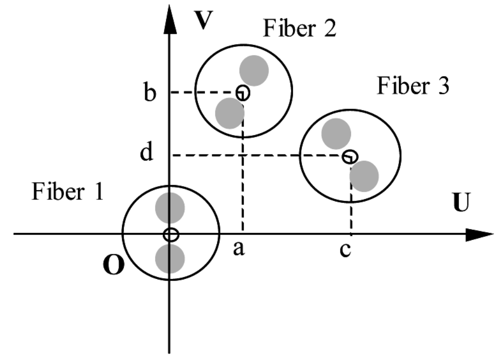

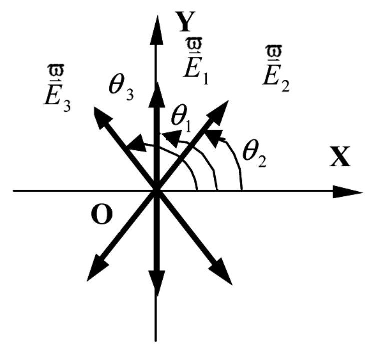

Fig. 1. (a) Three fiber core center position coordinate and (b) its polarization orientation angle coordinate.

Manuscript received July 7, 2007; revised December 13, 2007; accepted January 3, 2008. Published July 16, 2008 (projected). This work was supported in part by the National Natural Science Foundation of China under Grant 60577005 and in part by the Specialized Research Fund for the Doctoral Program of Higher Education Institute of MOE, China, to Harbin Engineering University. The associate editor coordinating the review of this paper and approving it for publication was Dr. Andrea Cusano.

The authors are with the Photonics Research Center, College of Science, Harbin Engineering University, Harbin 150001, China (e-mail: lbyuan@vip.sina.com).

Color versions of one or more of the figures in this paper are available online at http://ieeexplore.ieee.org.

Digital Object Identifier 10.1109/JSEN.2008.926974

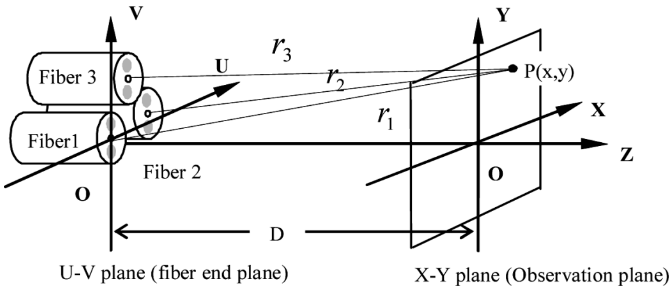

Fig. 2. Arrangement of fiber-optic grid generators' three fiber ends plane (UOV plane) and the observation plane (XOY plane).

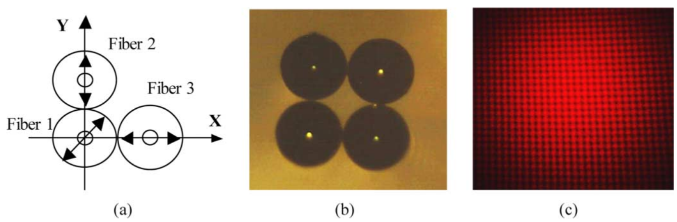

Fig. 3. Arrangement and interferometric grid pattern of three PM fiber formed a right angle isosceles triangle with polarization state of fiber 2 and 3 is orthogonal, while the polarization state of fiber 1 is at an angle of 45° with fiber 2 and fiber 3. (a) Arrangement of the three PM fiber; (b) implemented by using four fibers stacking and only fiber 1, 2, and 3 has been used; and (c) interferometric grid pattern of the three PM fiber.

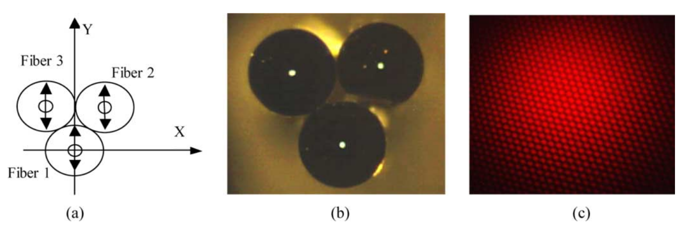

Fig. 4. Arrangement and interferometric grid pattern of three PM fiber formed an equilateral triangle with orientation of the three PM fibers polarization in the same direction. (a) Arrangement of the three PM fiber, (b) implemented by three fibers stacking, and (c) interferometric grid pattern.

where I_1, I_2 and I_3 are the light intensity of fiber 1, 2, and 3 at point $P(x, y)$. a, b, c and d are the coordinate values of fiber 2 and fiber 3 in UOV plane. λ is the light wavelength and D is the distance between fiber end plane and the observation plane. δ_{21}, δ_{31} and δ_{32} are the initial related phase difference between fiber 1 and 2, 3 and 1, and 3 and 2, respectively.

In order to implement the three PM fiber grid pattern generator, first, the three-fiber or four-fiber stacking technique has been used for making the fiber bundle; then, an epoxy is used to fix fibers; finally, a rotating cut method has been developed for fabricating the three PM fiber ends. By the rotation cutting methodology, each end surface of the three or four fibers can be controlled in the same plane. And the separate distance can be controlled less than 2–3 micrometer in the close stacking stage as shown in Figs. 3(b) and 4(b).

A. Design of Square Grid Pattern by Three PM Fiber

The three PM fibers ends are arranged in apexes of a right angle isosceles triangle as shown in Fig. 4. In this case, the coordinate of the three fiber center positions are $\mathrm{F}_1(0,0), \mathrm{F}_2(2r_0, 0)$ and $\mathrm{F}_3(0, 2r_0)$, where, r_0 is the radius of the PM fiber. The output optical field polarizations states of the three PM fibers are shown in Fig. 3. If the orientation of the three PM fiber polarization states is arranged as that the polarization direction of fiber 3 along X direction, fiber 2 along Y direction and fiber 1 polarization direction between X and Y axial at angle of 45° [Fig. 3(a)], then, the intensity of the three fiber interference grid fields can be simplified as

$$I(x,y) = I_1 + I_2 + I_3 + \sqrt{2I_1 I_2}\cos\left\{\frac{4\pi}{\lambda D} r_0 x - \delta_{21}\right\} + \sqrt{2I_1 I_3}\cos\left\{\frac{4\pi}{\lambda D} r_0 y - \delta_{31}\right\}. \quad (2)$$

From (2), it can be seen that there are two family interference fringes corresponding to the two coherence items. The grid pattern is given by Fig. 3(c).

B. Design of Hexagonal Grid Pattern

If the three PM fibers are arranged as an equilateral triangle, the coordinate of the three fiber core center positions are $\mathrm{F}_1(0,0), \mathrm{F}_2(r_0, \sqrt{3}r_0)$ and $\mathrm{F}_3(-r_0, \sqrt{3}r_0)$, as shown in Fig. 4. There are two equivalent arrangements for the polarization states of the three fibers. One case is all three fibers polarization states in the same direction [see Fig. 4(a)]; another case is at an angle of 120° to each other. In any case, the hexagonal grid pattern is all the same but the visibilities, as shown in Fig. 4(c). And the intensity of the three fiber interference grid fields can be given by

$$\begin{aligned} I(x,y) = I_1 + I_2 + I_3 &+ 2\sqrt{I_1 I_2}\cos\left\{\frac{2\pi r_0}{\lambda D}(x + \sqrt{3}y) - \delta_{21}\right\} \\ &+ 2\sqrt{I_1 I_3}\cos\left\{\frac{2\pi r_0}{\lambda D}(\sqrt{3}y - x) - \delta_{31}\right\} \\ &+ 2\sqrt{I_2 I_3}\cos\left\{\frac{4\pi r_0}{\lambda D} x + \delta_{32}\right\}. \quad (3) \end{aligned}$$

From (3), it can be seen that there are three family interference fringes corresponding to the three coherence items, corresponding to the hexagonal grid pattern.

III. Fourier Transform Method of GRID Pattern Analysis

The Fourier transform method of the fringe pattern analysis is successfully used for extracting phase information from fringe patterns caused by the interference of tilted wavefronts [12], [18], [19]. For the case of interference fringe pattern generated by the three PM fiber grid pattern generators, the arrangement of 3-D shape measuring system is described in Fig. 5. The measured object is on the XOY plane, and the CCD camera is amounted on the above of the object along the Z axial with distance H. The angle between fiber grid generator and the CCD

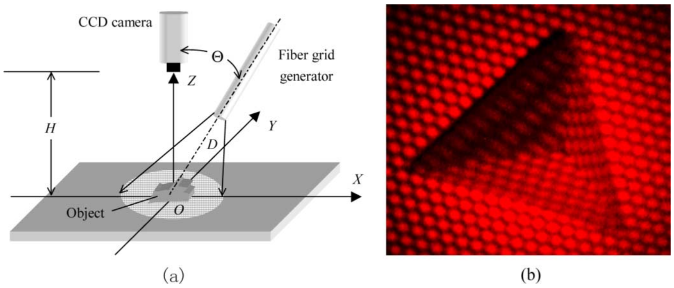

Fig. 5. Experimental setup of the three-fiber grid pattern based shape-sensing system. (a) Relative positions of fiber, object and CCD and (b) modulated hexagonal grid pattern by a triangle pyramid.

camera is Θ. Thus, the intensity distribution and the spatial carrier frequency objected to the XOY plane should be changed in X direction

$$\begin{aligned} I(x,y) = I_1 + I_2 + I_3 & \\ & + 2\sqrt{I_1 I_2}\cos\Theta\cos(\theta_1-\theta_2)\cos \\ & \times\left\{\frac{2\pi}{\lambda D}\left(\frac{a}{\cos\Theta}x+by\right)-\delta_{21}\right\} \\ & + 2\sqrt{I_1 I_3}\cos\Theta\cos(\theta_1-\theta_3)\cos \\ & \times\left\{\frac{2\pi}{\lambda D}\left(\frac{c}{\cos\Theta}x+dy\right)-\delta_{31}\right\} \\ & + 2\sqrt{I_2 I_3}\cos\Theta\cos(\theta_2-\theta_3)\cos \\ & \times\left\{\frac{2\pi}{\lambda D}\left[\frac{(c-a)}{\cos\Theta}x+(d-b)y\right]-\delta_{32}\right\}. \end{aligned} \tag{4}$$

The reflective grid pattern detected by the CCD camera is that the high spatial carrier frequencies are generated by the fiber grid pattern generator and the carrier frequency modulated by the object shape. It can be described by

$$\begin{aligned} & I_D(x,y) \\ & \quad = A(x,y) + B_1(x,y)\cos \\ & \qquad \times\{2\pi f_{0x1}x + 2\pi f_{0y1}y + \varphi_1(x,y)\} \\ & \qquad + B_2(x,y)\cos\{2\pi f_{0x2}x + 2\pi f_{0y2}y + \varphi_2(x,y)\} \\ & \qquad + B_3(x,y)\cos\{2\pi f_{0x3}x + 2\pi f_{0y3}y + \varphi_3(x,y)\} \end{aligned} \tag{5}$$

where the constant phase initial angles δ_{21}, δ_{31} and δ_{32} have been dropped and $A(x,y) = R(x,y)[I_1 + I_2 + I_3]$ is the unwanted background intensity, $R(x,y)$ represents the reflectivity distribution of the object surface and the reference plane XOY. $B_1(x,y), B_2(x,y)$ and $B_3(x,y)$ are the modulation terms, respectively. f_{0xi} and $f_{0yi} (i = 1,2,3)$ are the spatial carrier frequencies components in X direction and Y direction, respectively, which is introduced and determined by the fiber grid generator, where

$$\begin{cases} f_{0x1} = a/(\lambda D\cos\Theta) \\ f_{0x2} = c/(\lambda D\cos\Theta) \\ f_{0x3} = (c-a)/(\lambda D\cos\Theta) \end{cases} \qquad \begin{cases} f_{0y1} = b/(\lambda D) \\ f_{0y2} = d/(\lambda D) \\ f_{0y3} = (d-b)/(\lambda D) \end{cases} \tag{6}$$

and the phases $\varphi_1(x,y), \varphi_2(x,y)$ and $\varphi_3(x,y)$ contains the desired information, which is modulated phase by the object surface shape.

The principal problem in the pattern analysis is how to obtain the phase information $\varphi_1(x,y), \varphi_2(x,y)$ and $\varphi_3(x,y)$ from a given modulated grid pattern, by separating it from other terms $A(x,y)$ and $B_1(x,y), B_2(x,y)$ and $B_3(x,y)$. This can be done by using 2-D Fourier transform [20], [21]. For the purpose of 2-D Fourier pattern analysis, the input pattern can be conveniently written in the following form:

$$\begin{aligned} I_D(x,y) = A(x,y) &+ C_1(x,y)e^{i2\pi(f_{0x1}x+f_{0y1}y)} \\ &+ C_1^*(x,y)e^{-i2\pi(f_{0x1}x+f_{0y1}y)} \\ &+ C_2(x,y)e^{i2\pi(f_{0x2}x+f_{0y2}y)} \\ &+ C_2^*(x,y)e^{-i2\pi(f_{0x2}x+f_{oy2})} \\ &+ C_3(x,y)e^{i2\pi(f_{0x3}x+f_{0y3}y)} \\ &+ C_3^*(x,y)e^{-i2\pi(f_{0x3}x+f_{0y3}y)} \end{aligned} \tag{7}$$

where $C_i(x,y) = (1)/(2)B_i(x,y)e^{i\varphi_i(x,y)} (i = 1,2,3)$ and the asterisk denotes complex conjugation.

The Fourier transform $F(f_{x1}, f_{x2}, f_{x3}, f_{y1}, f_{y2}, f_{y3})$ of recorded pattern intensity distribution $I_D(x,y)$ is given by

$$\begin{aligned} & F(f_{x1}, f_{x2}, f_{x3}, f_{y1}, f_{y2}, f_{y3}) \\ & \quad = \Lambda(f_{x1}, f_{x2}, f_{x3}, f_{y1}, f_{y2}, f_{y3}) + \\ & \qquad + Q_1(f_{x1} - f_{0x1}, f_{y1} - f_{0y1}) \\ & \qquad + Q_1^*(f_{x1} + f_{0x1}, f_{y1} + f_{0y1}) \\ & \qquad + Q_2(f_{x2} - f_{0x2}, f_{y2} - f_{0y2}) + \\ & \qquad + Q_2^*(f_{x2} + f_{0x2}, f_{y2} + f_{0y2}) \\ & \qquad + Q_3(f_{x3} - f_{0x3}, f_{y3} - f_{0y3}) \\ & \qquad + Q_3^*(f_{x3} + f_{0x3}, f_{y3} + f_{0y3}). \end{aligned} \tag{8}$$

Assume that the distribution functions $A(x,y)$ and $B_i(x,y)$, $(i = 1,2,3)$ and the phases $\varphi_i(x,y), (i = 1,2,3)$ change very slowly compared with the carrier frequency f_{0xi} and $f_{0yi} (i = 1,2,3)$. All the spectra are separated from each other by the carrier frequency f_{0xi} and $f_{0yi} (i = 1,2,3)$. One of the side peaks is weighted by the Hanning window and translated by f_{0xi} and $f_{0yi} (i = 1,2,3)$ towards the origin to obtain $Q_i(f_{xi}, f_{yi}), (i = 1,2,3)$. The unwanted background variation $\Lambda(f_{x1}, f_{x2}, f_{x3}, f_{y1}, f_{y2}, f_{y3})$ and the central peak and the six side peaks are filtered out on this stage. Taking the inverse Fourier transform of $Q_i(f_{xi}, f_{yi}), (i = 1,2,3)$ with respect to $(f_{xi}, f_{yi}), (i = 1,2,3)$ and obtained $C_i(x,y)$. Thus the phase $\varphi_i(x,y)$ in the imaginary part is completely separated from the amplitude variation $B_i(x,y)$ in the real part

$$\varphi_i(x,y) = \arctan\left\{\frac{\mathrm{Re}\,[C_i(x,y)]}{\mathrm{Im}\,[C_i(x,y)]}\right\}, (i = 1,2,3) \tag{9}$$

where $\mathrm{Re}[C_i(x,y)]$ and $\mathrm{Im}[C_i(x,y)]$ denote the real and imaginary part of $C_i(x,y)$, respectively. Since phase calculation by the computer gives principal values ranging from $-\pi$ to π, the phase distribution is wrapped into this range and, consequently, has discontinuities with 2 π phase jumps for variations larger than 2 π. Therefore, phase unwrapping schemes are required to

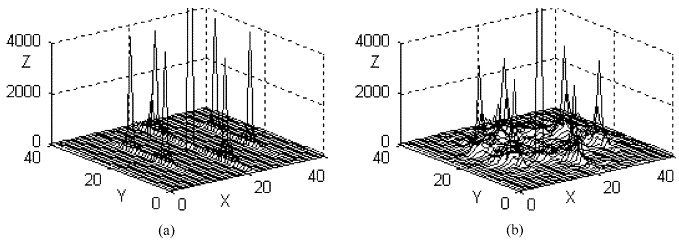

Fig. 6. Fourier spectra of hexagonal grid pattern of Fig. 4(c) and Fig. 5(b). (a) Fourier spectra without modulation. (b) Fourier spectra modulation by a triangle pyramid.

produce a continuous phase distribution [22]–[24] It can be corrected easily by adding or subtracting 2 π according to the phase jump ranging from - π to π or *vice versa*.

IV. Experimental Results

A schematic diagram of the experimental system is shown in Fig. 5. Light from a 8 mW laser diode (LD) at wavelength $\lambda = 650$ nm was launched into a single-mode fiber and polarized by an in-line polarizer and then collimated by a GRIN lens impinged upon the three fiber grid pattern generator. The distance between the fiber end and the object is $\mathrm{D} = 155$ mm, and the angle Θ between the fiber grid pattern generator and the CCD camera is 45°, the height is $\mathrm{H} = 150$ mm, and the size of the triangle pyramid is 15 mm for each egad length of the bottom surface with 7.5 mm high. The interference grid patterns of hexagonal modulated by the triangle pyramid is shown in Fig. 5(b). To demonstrate the fiber-optic grid interferogram shape sensing performance, a triangle pyramid is chosen as the test object. The three-fiber grid pattern generator has generated the square and hexagonal grid pattern with the higher carrier frequency as shown in Figs. 3(c) and 4(c). The Fourier transform results of the fiber-optic grid interferogram before and after modulated by the triangle pyramid are given in Figs. 6(a) and (b), respectively, which corresponding the 2-D Fourier spectra of carrier frequency without modulated and modulated case. There are three pair (total six) spatial frequency side peaks for hexagonal grid pattern as plotted in Fig. 6, and the three independent orientation and three independent side peak can be used to reconstructed the triangle pyramid surface. It is obvious that each individual $\varphi_i(x,y)$ of the three phases given by (9) could be used to reconstruct the shape of the measured object. So that three independent reconstruction shape surface of the measured object could be obtained. It presents the three independent carrier frequencies modulated by the same object from different orientations. This information redundancy has the advantages both in data fusion to improve the measuring accuracy and the analysis method modification for the sharper parts of the object surface. For example, the simple data fusion may be described as the average of the three phases

$$\varphi(x,y) = \frac{1}{3}\sum_{i=1}^{3}\varphi_i(x,y). \tag{10}$$

By this data fusion method, the sharper parts of the object surface of the phase has been greatly improved. The height of the

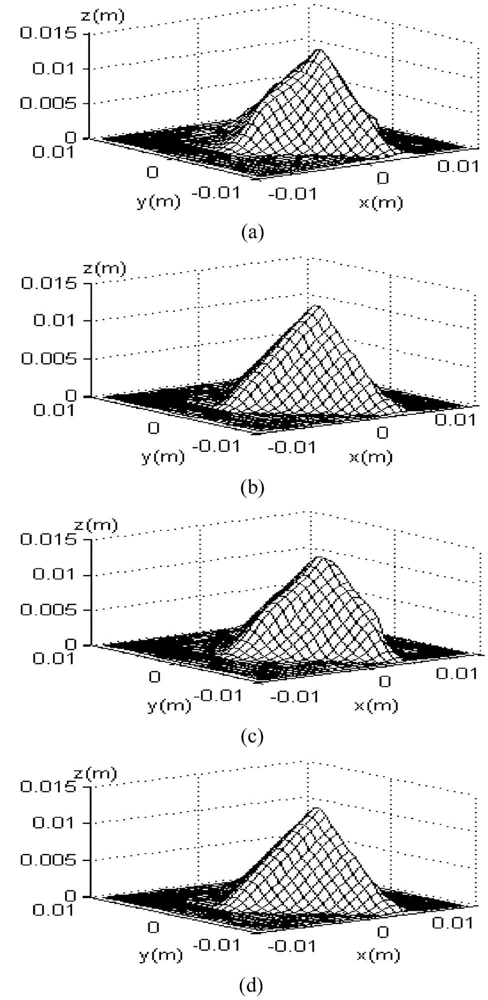

Fig. 7. Experimental results of the triangle pyramid reconstruction. (a) Reconstructed in orientation 1 by phase $\varphi(x,y)_1$, (b) reconstructed in orientation 2 by phase $\varphi(x,y)_2$, (c) reconstructed in orientation 3 by phase $\varphi(x,y)_3$, and (d) reconstructed by phase data fusion $\varphi(x,y) = \Sigma\varphi_i, (i = 1,2,3)$.

object is encoded in the phase of the pattern, and it can be retrieved by the 2-D Fourier transform method. The reconstructed triangle pyramid shape surface in our experiment is given by Fig. 7(a)-(c). The improvement of the measuring accuracy by three phases data fusion is illustrated in Fig. 7(d).

A comparison of the results shows that the root-mean-squared (rms) error is 0.21 mm, or 3.1% of the object depth. This is good agreement with the relationship that exists between the number of fringes and rms error [25]. This error figure seems to be quite high for the sensitivity of the system, when compared to similar results in previously published work [26], [27]. However, these are the preliminary results and are aimed to prove that the proposed three-fiber grid pattern generating scheme in optical profilometry is promising. The error margin can be easily reduced by redesigning the three-fiber separate distance for desired grid spacing.

V. Conclusion

In conclusion, a three-PM fiber based optic shape sensing system has been proposed and demonstrated. By using the fiber-optic grid interferogram technique, it is greatly simplified the holographic interferometry system. The carrier grid interferogram can be conveniently generated without the use of excessive auxiliary components or sophisticated experimental devices, and moreover, it can be used in very narrow places due to its small size. The advantage of the fiber-optic grid interferogram generation method used here is simplicity in experimental realization. The 2-D Fourier transform method of the fiber-optic grid interferogram pattern analysis is successfully used for extracting phase information from the modulated pattern generated by the fiber grid pattern generator. The multiphase data fusion method has been used in our experiments, which greatly improved the accuracy of the 3-D shape measuring results. For example, a small triangle pyramid has been used to demonstrate how to reconstruct the three-dimensional shape by the fiber-optic grid interferogram technique.

REFERENCES

[1] H. Takasaki, "Generation of surface contours by moiré pattern," *Appl. Opt.*, vol. 9, no. 4, pp. 942–947, 1970.
[2] T. Yoshizawa, "The recent trend of moiré metrology," *J. Robust. Mech.*, vol. 3, no. 3, pp. 80–85, 1991.
[3] V. Srinivasan, H. C. Liu, and M. Halioua, "Automated phase measuring profilometry of 3-D diffuse object," *Appl. Opt.*, vol. 23, no. 18, pp. 3l05–3108, 1984.
[4] X.-Y. Su, W.-S. Zhou, V. von Bally, and D. Vukicevic, "Automated phase-measuring profilometry using defocused projection of a Ronchi grating," *Opt. Commun.*, vol. 94, no. 6, pp. 561–573, 1992.
[5] X.-Y. Su, G. von Bally, and D. Vukicevic, "Phase-stepping grating profilometry: Utilization of intensity modulation analysis in complex objects evaluation," *Opt. Commun.*, vol. 98, no. 1, pp. 141–150, 1993.
[6] W.-S. Zhou and X.-Y. Su, "A direct mapping algorithm for phase-measuring profilometry," *J. Mod. Opt.*, vol. 41, no. 1, pp. 89–93, 1994.
[7] J. L. Li, X. Su, and H. J. Su, "Removal of carrier frequency in phase-shifting techniques," *Opt. Lasers Eng.*, vol. 30, no. 1, pp. 107–115, 1998.
[8] J. Li, X. Su, and H. Su, "New PMP method with two-frequency grating projection," *Proc. SPIE*, vol. 2778, pp. 481–482, 1996.
[9] X. Lian and X. Su, "Computer simulation of a 3-D sensing system with structured illumination," *Opt. Laser Eng.*, vol. 27, pp. 379–393, 1997.
[10] J. Li, H. Su, and X. Su, "Two-frequency grating used in phase-measuring profilometry," *Appl. Opt.*, vol. 36, no. 1, pp. 277–280, 1997.
[11] H. Zhang, M. J. Lalor, and D. R. Burton, "Spatial temporal phase unwrapping for the measurement of discontinuous objects in dynamic fringe-projection phase-shifting profilometry," *Appl. Opt.*, vol. 38, no. 16, pp. 3534–3541, 1999.
[12] M. Takeda, H. Ina, and S. Koboyashi, "Fourier-transform method of fringe-pattern analysis for computer based topography and interferometry," *J. Opt. Soc. Amer.*, vol. 72, no. 1, pp. 156–160, 1982.
[13] M. Takeda and K. Motoh, "Fourier transform profilometry for the automatic measurement of 3-D object shapes," *Appl. Opt.*, vol. 22, no. 24, pp. 3977–3982, 1983.
[14] X. Su and L. Su, "New 3D profilometry based on modulation measurement," *Proc. SPIE*, vol. 3558, pp. 1–7, 1998.
[15] L. Su, X. Su, and W. Li, "Application of modulation measurement profilometry to objects with surface holes," *Appl. Opt.*, vol. 38, no. 7, pp. 1153–1158, 1999.
[16] L. B. Yuan, "Fiber optic Moiré interferometer," *Chinese Phys. Lett.*, vol. 14, pp. 675–677, 1997.
[17] L. B. Yuan and L. M. Zhou, "Fiber optic Moiré interference principle," *Opt. Fiber Technol.*, vol. 4, pp. 224–232, 1998.
[18] R. J. Green, J. G. Walker, and D. W. Robinson, "Investigation of the Fourier-transform method of fringe pattern analysis," *Opt. Lasers Eng.*, vol. 8, pp. 29–44, 1988.
[19] T. R. Judge, C. Quan, and P. J. Bryanston-Cross, "Holographic deformation measurements by Fourier-transform technique with automatic phase unwrapping," *Opt. Eng.*, vol. 31, pp. 533–543, 1992.
[20] W. W. Macy, "Two-dimensional fringe-pattern analysis," *Appl. Opt.*, vol. 22, no. 23, pp. 3898–3901, 1983.
[21] D. J. Bone, H. A. Bachor, and R. J. Sandeman, "Fringe-pattern analysis using a 2-D Fourier transform," *Appl. Opt.*, vol. 25, pp. 1653–1660, 1986.
[22] M. O. Petersen, "Phase map unwrapping: A comparison of some traditional methods and a presentation of a new approach," *Proc. SPIE*, vol. 1508, pp. 73–82, 1991.
[23] J. M. Huntley and H. Saldner, "Temporal phase-unwrapping algorithm for automated interferogram analysis," *Appl. Opt.*, vol. 32, no. 17, pp. 3047–3052, 1993.
[24] T. Kreis, "Digital holographic interference-phase measurement using the Fourier transform method," *J. Opt. Soc. Amer.*, vol. 3, pp. 847–855, 1986.
[25] F. Berryman, P. Pynsent, and J. Cubillo, "The effect of windowing in Fourier transform profilometry applied to noisy images," *Opt. Lasers Eng.*, vol. 41, no. 6, pp. 815–826, 2004.
[26] G. S. Spagnolo, G. Guattari, C. Sapia, D. Ambrosini, D. Paoletti, and G. Accardo, "Three-dimensional optical profilometry for artwork inspection," *J. Opt. A-Pure Appl. Opt.*, vol. 2, pp. 353–361, 2000.
[27] T. L. Pennington, H. Xiao, R. May, and A. Wang, "Miniaturized 3-D surface profilometer using a fiber optic coupler," *Opt. Laser Technol.*, vol. 33, pp. 313–320, 2001.

Libo Yuan, photograph and biography not available at the time of publication.

Yanlei Liu, photograph and biography not available at the time of publication.

Zhihai Liu, photograph and biography not available at the time of publication.

Xiaoyan Lin, photograph and biography not available at the time of publication.